Hindawi
Advances in Materials Science and Engineering
Volume 2021, Article ID 2809370, 15 pages
https://doi.org/10.1155/2021/2809370

Research Article

Strain-Softening Characteristics of Hydrate-Bearing Sediments and Modified Duncan–Chang Model

Mengqiu Yan, Rongtao Yan, and Haihao Yu

College of Civil Engineering and Architecture, Guilin University of Technology, Guangxi Key Laboratory of Geomechanics and Geotechnical Engineering, Guilin, Guangxi 541004, China

Correspondence should be addressed to Rongtao Yan; 2012019@glut.edu.cn and Haihao Yu; 2018094@glut.edu.cn

Received 13 November 2021; Accepted 3 December 2021; Published 17 December 2021

Academic Editor: Yonghong Wang

Copyright © 2021 Mengqiu Yan et al. This is an open access article distributed under the Creative Commons Attribution License, which permits unrestricted use, distribution, and reproduction in any medium, provided the original work is properly cited.

Marine hydrate exploitation may trigger the seabed geological disaster, such as seafloor collapse and landslide. It is critically important to understand the mechanical properties of hydrate-bearing sediment. Strain-softening observation is a typical behavior of hydrate-bearing sediment (HBS) and exhibits more significant at higher hydrate saturation. This paper performed a series of triaxial compression tests on methane hydrate-bearing sand to analyze the influence rule and mechanism of hydrate saturation on the strain-softening characteristic, stiffness, and strength and introduced the strain-softening index to quantificationally characterize the strain-softening behaviors of HBS with different hydrate saturations. Based on the analyses on the mechanical behavior of HBS, the Duncan–Chang model is extended to address the stress-strain curves of HBS. Two empirical formulas with hydrate saturation embedded are used to characterize the enhanced initial modulus and strength for HBS, respectively. To address the strain-softening behavior of HBS, the modified Duncan–Chang model introduced a damage factor into the strength of HBS. To validate the modified Duncan–Chang model, four different triaxial compression tests are simulated. The good consistence between simulated result and experimental data demonstrates that the modified Duncan–Chang model is capable of reflecting the influence of hydrate saturation not only on the stiffness and strength but also on the strain-softening characteristics of HBS.

1. Introduction

Methane hydrate is an ice-like clathrate compound formed by methane and water at the relative high pressure and low temperature. In nature, methane hydrate mainly distributes in the deep sea continental shelf area and high-latitude permafrost [1–3]. The methane hydrate is often considered as an alternative energy because the huge reserves exist all over the world [2, 4, 5]. The current commonly accepted exploitation method for hydrate is to dissociate the methane hydrate back into methane and water and then extract the methane from the reservoir. The dissociation method includes heating, depressurization, and inhibitor injection [6, 7]. However, the hydrate dissociation could reduce the strength of hydrate-bearing sediments (HBS), perhaps causing the submarine landslide during hydrate exploitation [7–10]. Therefore, the study on the mechanical properties of HBS is necessary. Moreover, developing a robust and simple constitutive model is also important for the safe exploitation of methane hydrate [11–13].

To reveal the effects of hydrate on the mechanical behaviors of HBS, several researchers have performed a lot of laboratory tests. Hyodo et al. [8] synthesized methane hydrate-bearing sandy sediments using the excess gas method and carried out a series of triaxial compression tests to study the effects of effective confining pressure, porosity, pore pressure, and temperature on the shear properties. Yoneda et al. [14] tested the mechanical behaviors of undisturbed specimen of hydrate-bearing sediment and compared to the artificial hydrate-bearing sediment specimen. The result demonstrated that both have similar stiffness and strength characteristics. Liu et al. [15] carried out direct shear tests on CO_2 hydrate-bearing sediments, which showed that both of the peak strength and residual strength increase with the

increasing hydrate saturation and vertical stress. Yoneda et al. [16] carried out isotropic compression tests on hydrate-bearing pressure-core sediments recovered from the Krishna-Godavari Basin, offshore India. The result showed that the presence of hydrate reduces the compression index and swelling index. Through the triaxial shear test of methane hydrate-bearing sediments with different fine particle contents, Hyodo et al. [17] suggested that the shear strength and dilatancy of HBS increase significantly with the increase of fine particle content. Overall, the increasing hydrate saturation could enhance the stiffness, strength, strain-softening behavior, and dilation of HBS [18].

To characterize these mechanical behaviors of HBS, several of elastoplastic constitutive models have been developed. Uchida et al. [19] proposed an elastoplastic constitutive model for HBS in the framework of critical state soil mechanics, which effectively captures the enhanced stiffness, strength, strain-softening, and dilatancy of HBS. Based on the thermodynamic theory, Sun et al. [20] developed the critical state constitutive model of HBS. The enhanced strain softening and dilatancy of HBS are satisfactorily addressed. To address the effects of hydrate saturation, confining pressure, and density on mechanical behaviors of HBS, Shen et al. [21] proposed a state-dependent critical state model. In addition, Yan and Wei [22], Sanchez et al. [23], and Sun et al. [11] also developed the elastoplastic constitutive models for HBS. On the whole, all these models have great ability to predict the typical mechanical behaviors of HBS. However, the theories and formulas for these models are complicated, which limits the application in the hydrate-related geotechnical engineering problems.

The Duncan–Chang model is a nonlinear elastic constitutive model widely used in the engineering practices. Through summarizing the fundamental features of stress-strain curve of soil, the Duncan–Chang model was derived. The theory and formulas for the Duncan–Chang model are simple and easy to understand for the engineers. Recently, the Duncan–Chang model is used to address the mechanical behaviors of HBS. According to the triaxial compression results, Miyazaki et al. [24, 25] related the strength and stiffness to the hydrate saturation and confining pressure and modified the formulas of strength and stiffness for extending the original Duncan–Chang model to address the mechanical behaviors of HBS. The modified Duncan–Chang model is able to effectively describe the stress-strain relationship of HBS with different hydrate saturations. Through analyzing the stress-strain curve of HBS, the Duncan–Chang model was extended by Yu et al. [26] to address the mechanical behaviors of HBS at different temperatures, confining pressure, and strain rate. To reflect the influences of dissociation time and dissociation temperature on the mechanical properties of HBS, Song et al. [27] also modified the Duncan–Chang model. All these modified Duncan–Chang nonlinear elastic models have the ability of capturing the enhanced strength and stiffness of HBS, but the strain-softening characteristic of HBS cannot be addressed.

To comprehensively understand the strain-softening characteristic of HBS, a series of triaxial compression tests are performed on methane hydrate-bearing sand. Meanwhile, the Duncan–Chang model is modified to address the strain-softening characteristic of HBS. Finally, the modified Duncan–Chang model is capable of simulating the enhanced stiffness, strength, and strain-softening characteristic of HBS, which could have an important academic and engineering significance for methane hydrate exploitation.

2. Experimental Illustrations

2.1. Apparatus Introduction. An innovative temperature-controlled high-pressure triaxial testing apparatus with the capacity to reproduce subsea floor reservoir conditions is employed in this experimental study. Figure 1 shows the triaxial testing apparatus for HBS. The HBS sample is placed in the high-pressure reactor that can provide the maximum confining pressure of 30 MPa with the accuracy of 0.1% F.S. through a servo pump. The other two servo pumps are linked to the sample pores and provide the pore pressure and back pressure. The capacity of pump is 30 MPa and the accuracy is 0.1% F.S. The axial loading element provides a maximum pressure of 35 MPa with an accuracy of 0.1% F.S. Through immersing the high-pressure chamber into the bath of the temperature control component, the temperature of the sample is adjusted between −25°C and 50°C by circulating the ethylene glycol solution. The control accuracy for the temperature is ±0.1°C. The computer is used to collect the experimental data and control the text process through the data processing component.

2.2. Test Material and Sample Preparation. The host sediment used in this study is sand, with a particle size ranging from 0.075 mm to 0.25 mm and the gravity *Gs* of 2.65. The gas for synthesizing hydrate is methane, which is bought from the Huate Gas Co. Ltd., Foshan, China, with the purity of 99.99%.

This study adopted the "excess gas method" to synthesize methane hydrate in sandy sediments [28]. Generally, the initial water content of the sample before hydrate formation controls the hydrate saturation [28]. According to the target of the hydrate saturation, the predetermined water is mixed completely with the sand. After waiting 24 hours for water distribution uniformly within the sample, the wet sand is compacted into four layers in a cylindrical mold with the sample size of the height $H = 100$ mm and the diameter $D = 50$ mm. The dry density is set to be 1.6 g/cm^3. The images of the sample are shown in Figure 2. Sequently, the sample is transferred to the high-pressure reactor and placed on the pedestal. After installing the devices, the confining pressure of 0.2 MPa is applied to ensure the sample stand stable. Then, the methane gas is increased up to 8.0 MPa with the constant net effective confining pressure of 0.2 MPa. Immersing the high-pressure reactor into the water bath, the temperature is lowered down to 2°C for methane hydrate formation. Due to the methane consumption for hydrate synthesis, the decrease in methane pressure can be observed. When the methane pressure drops to a certain value and the change in 8 hours is less than 0.01 MPa, the hydrate formation is

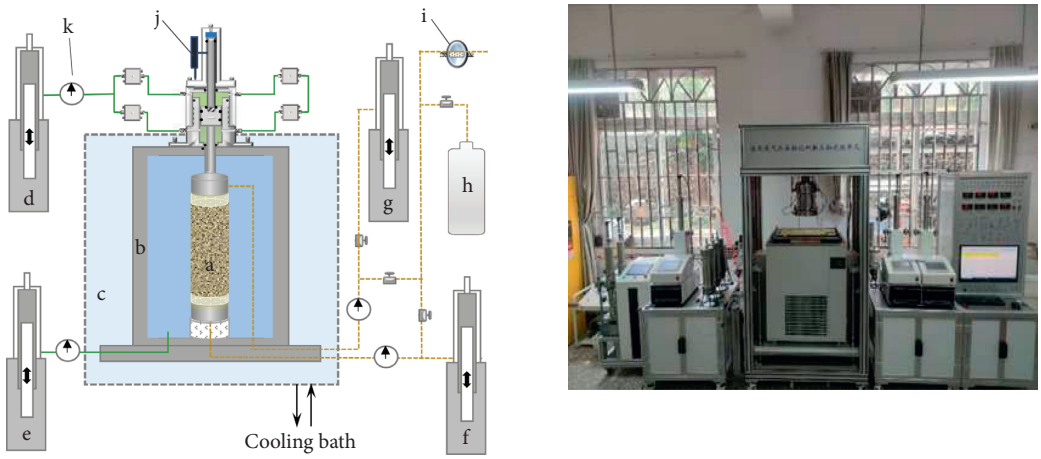

(a) Specimen (b) High pressure reactor (c) Water bath
(d) Loading pump (e) Confining pump (f) Pore pressure pump
(g) Back pump (h) Methane gas (i) Gas flow meter
(j) Displacement transducer (k) Pressure transducer

(a) (b)

Figure 1: The triaxial testing apparatus for HBS. (a) Schematic diagram. (b) Real diagram.

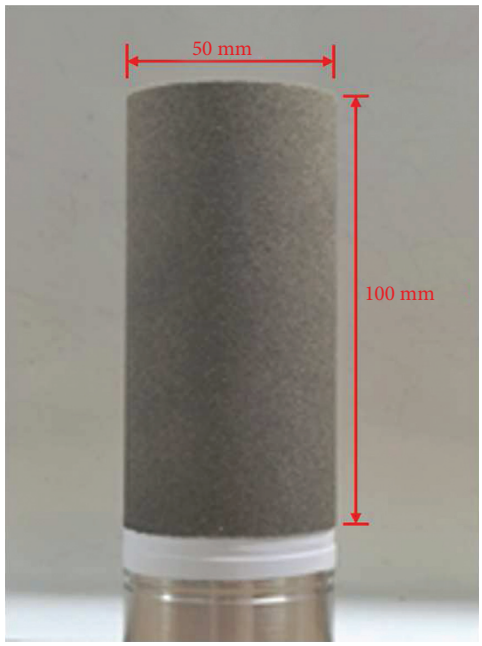

Figure 2: Image of triaxial test sample.

viewed as completed. According to the methane amount consumed in the hydrate formation, the hydrate saturation is calculated based on the gas state equation. The formula for hydrate saturation is given by [29]

$$S_h = \frac{V_h}{V_p} = \frac{\left(PV_g/ZRT\right) \cdot M_h}{\rho_h \cdot V_p}, \quad (1)$$

where S_h is the hydrate saturation, V_h is the volume of the hydrate, V_p is the volume of the pore space in the sample, M_h is the molar mass of hydrate, the value is 125.934 g/mol (calculated from the hydration number 6.1) [30], P is the pore pressure, T is the generation temperature, Vg is the volume of CH_4 gas, Z is the compressibility factor of CH_4 gas, and ρ_h is the density of CH_4 hydrate (0.917 g/cm^3) [31].

2.3. Triaxial Compression Procedure. The triaxial compression tests are carried out on the formed hydrate-bearing sandy sediment. The shear mode is consolidated and drained shear. During the shear tests, the effective confining pressure is set to be 1, 3, and 5 MPa, respectively, with the pore pressure of 8 MPa. The volume contraction occurs during the consolidation stage. The consolidation is considered as completed once the change in volumetric strain is less than 0.05% per hour. Then, the shear begins with the axial loading rate of 0.02 mm/min and not stops until the axial strain reaches 20%. The detailed conditions for tests are shown in Table 1.

3. Results and Analyses

3.1. Stress-Strain Curves. The stress-strain curve reflects the mechanical characteristics of HBS, especially for deformation and strength. Figure 3 presents the stress-strain relationships of HBS with different hydrate saturations under different effective confining pressures ($\sigma_3' = 1$, 3, and 5 MPa). With the increase of hydrate saturation from 0% to ~33%, the strength and stiffness of HBS are greatly improved with different degrees. This is because that the hydrate bonds the soil particles and/or fills into the sediment pores, increasing the integrity of HBS [7]. This change in the strength and strength is observed in the previous research studies [18]. In the case of

Table 1: The test conditions for HBS specimens.

No.	Pore pressure (MPa)	Confining pressure (MPa)	Effective confining pressure (MPa)	Hydrate saturation S_h (%)
S0	8	9	1	0
		11	3	0
		13	5	0
S1	8	9	1	4.6
		11	3	4.3
		13	5	4.2
S2	8	9	1	9.6
		11	3	9.6
		13	5	9.1
S3	8	9	1	18.9
		11	3	18.8
		13	5	19
S4	8	9	1	33.5
		11	3	32.8
		13	5	32.4

$\sigma_3' = 1$ MPa, the stress-strain curves of HBS show a significant strain-softening behavior, which is more obvious at the higher hydrate saturation. When hydrate saturation $S_h = 0\%$, the pure sandy sample exhibits a strain-hardening behavior. As the effective confining pressure increases, the strain-softening behavior of HBS is suppressed. When $\sigma_3' = 3$ MPa, the samples with hydrate saturation of 18.8% and 32.8% show a strain-softening phenomenon, and the samples with hydrate saturation of 4.3% and 9.9% show a strain-hardening phenomenon. When $\sigma_3' = 5$ MPa, the sample with 32.4% hydrate saturation shows strain-softening, and the sample with 4.2%, 9.1%, and 19% hydrate saturation show strain-hardening. To further understand the strain-softening behaviors of HBS, a detailed analysis is made in the next section.

3.2. Strain-Softening Characteristics. According to the stress-strain curves of HBS, it can be found that the hydrate saturation and the effective confining pressure have remarkable influences on the strain-softening behaviors. To quantificationally analyze the strain-softening behaviors of HBS, a new concept, the strain-softening index D_s, is presented. The D_S is defined as the slope of the fitting straight line for the 3% stress-strain curve after the strength of HBS, shown in Figure 4. The formula for D_S is presented as follows:

$$\mathrm{D}_s = \frac{\Delta q}{\Delta \varepsilon_1}, \tag{2}$$

where $\Delta\varepsilon_1$ is the increment in axial strain. Generally, $\Delta\varepsilon_1$ is set to be 3% after the strength point of the stress-strain curve. Δq is the corresponding increment in deviatoric stress. The strength of HBS is determined according to the standard for the soil test method (GB/T 50123-2019) in China [32]. The strain-softening stress-strain curve shows a negative value of D_S, and the smaller Ds is, the greater the softening degree is. On the contrary, the strain-hardening stress-strain curve presents a positive value of D_S.

Figure 5 shows the relationship between strain-softening index D_S and hydrate saturation under different effective confining pressures ($\sigma_3' = 1$ MPa, 3 MPa, and 5 MPa). From Figure 5, the values of D_S for the case of $\sigma_3' = 1$ MPa are below the horizontal line of $D_S = 0$ except for the pure sandy sediment, but all the values of D_S for the case of $\sigma_3' = 5$ MPa are larger than zero. The values of D_S for the case of $\sigma_3' = 3$ MPa are between the cases of $\sigma_3' = 1$ MPa and $\sigma_3' = 5$ MPa. Apparently, the increasing effective confining pressure suppresses the strain-softening behavior of hydrate-bearing sediment.

For the different effective confining pressures, the hydrate saturation has a similar influence tendency. As the hydrate saturation increases, the values of D_s tend to decrease. For the case of $\sigma_3' = 1$ MPa, the hydrate-bearing sediment exhibits more significant strain-softening behaviors. Under $\sigma_3' = 5$ condition, however, the increasing hydrate saturation weakens the strain-hardening behavior. Clearly, the HBS sample can transfer the deformation model from strain-hardening to strain-softening with the increasing hydrate saturation.

As for hydrate-bearing sediment, hydrate occurrence could affect the mechanical behaviors of HBS only for the load bearing and cementation hydrate habits. Figure 6 presents the mechanism for the internal structure of the hydrate-bearing sediment during shearing for the load bearing and cementation habits. For the loading bearing, shearing action can drive the rolling, sliding, and rearrangement of soil particles [7, 33]. Since the hydrate hinders this movement, more force is required to make soil particle climbing over the other soil particles. Therefore, the strength of HBS is increased. However, the increased force also damages the hydrate particles, lowers down the integrality of HBS, and further gives rise to the strain-softening behaviors. As for cementation habit, hydrate occurs between the two soil particles and bonds the soil particles to increase the integrality. In the shear test, it needs to overcome the cementation before soil particles move each other. Thus, the strength of HBS increases with the increasing hydrate saturation. With the large enough shear stress, the hydrate could debond from the soil particles. Furthermore, the debond hydrate could be broken down and crushed. These hydrate damage mechanisms lead to the strain-softening behaviors of hydrate-bearing sediment [7, 33]. However, the

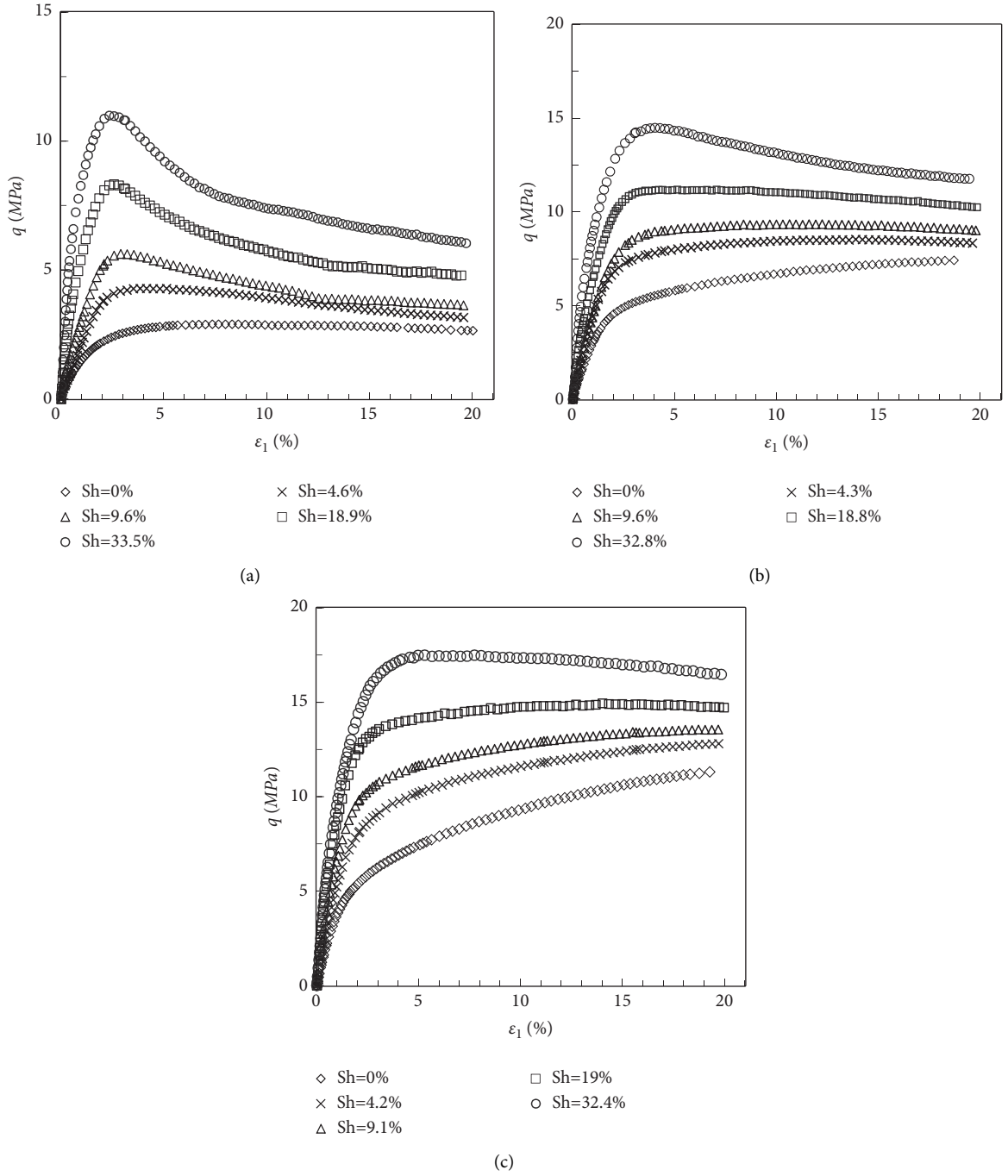

Figure 3: The stress-strain curves of hydrate-bearing sand: (a) $\sigma_3' = 1$ MPa, (b) $\sigma_3' = 3$ MPa, and (c) $\sigma_3' = 5$ MPa.

high effective confining pressure hinders the relative movement of soil and hydrate particle, and the sample mainly exhibits the volume contraction during the shear process. The denser structure of the sample prompts the strain-hardening behavior.

Based on the above analyses, hydrate damage and breakdown degraded the hydrate-bonding effect for both the load bearing and cementation, which mainly contributes to the strain-softening behaviors of HBS [7, 9]. Pinkert et al. [34] analyzed the strain-softening behaviors of HBS based on the decrease in hydrate saturation induced by the shear dilatation, but the hydrate saturation reduction is an important influence factor, not the essential reason. Therefore, in Section 4, the hydrate damage is considered as the main influence factor on the strain-softening behaviors of HBS for extending the Duncan–Chang constitutive model to address the strain-softening behaviors of HBS.

3.3. Stiffness and Strength. The stiffness and strength are the typical characteristics for evaluating the mechanical behaviors of HBS. Meanwhile, understanding the stiffness and

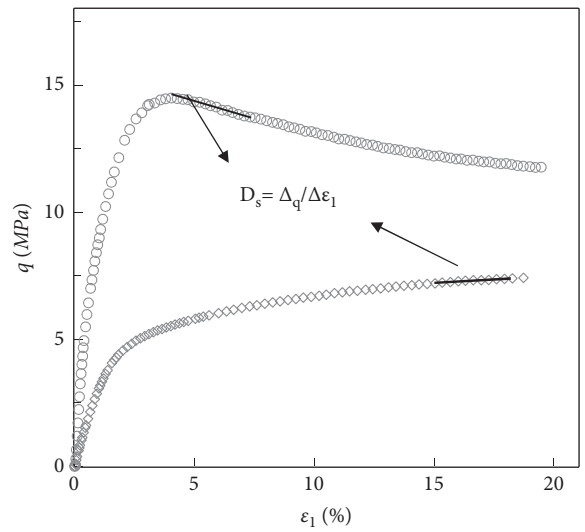

Figure 4: The schematic diagram for defining the strain-softening index.

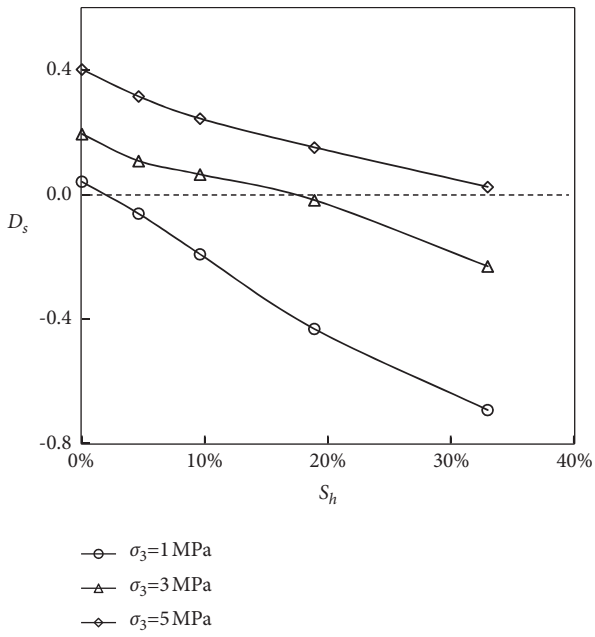

Figure 5: The relationship between the strain-softening index and hydrate saturation.

strength is benefit for developing the constitutive model for HBS. Thus, this section analyzes the stiffness and strength of HBS.

This paper selects the secant modulus of $\varepsilon_1 = 0 \sim 1\%$ as the representative to investigate the stiffness of HBS. The change in the secant modulus of HBS with hydrate saturation under different effective confining pressures is shown in Figure 7. With the increasing hydrate saturation, the secant modulus has a remarkable improvement, and the increased tendency of secant modulus with hydrate saturation could be characterized by the linear function. This is due to that the cementation or filling effect of hydrate within sediment pores increases the resistance to the relative movement of soil particles, leading to the enhanced stiffness of HBS. Figure 6 also presents the samples with higher effective confining pressure having a larger secant modulus at a given hydrate saturation. Due to the increase of the effective confining pressure, the contact area is enlarged, the increase of cracks is restrained, and the slip, overturning, and rearrangement between particles are prevented, thus increasing the friction resistance. As a result, the HBS sample has a greater stiffness [33].

Figure 8 shows the relationship between failure strength and hydrate saturation under different effective confining pressures. The failure strength is taken as the deviatoric stress at the peak point for a strain-softening curve or at the 15% axial strain for a strain-hardening curve. Figure 8 finds that the hydrate saturation and the effective confining pressure have apparent effects on the strength of HBS. The HBS sample with higher hydrate saturation and larger effective confining pressure has a higher failure strength. This observation is consistent with the previous experimental result [7, 18]. The reason is that the cementation of hydrate to the soil skeleton and the contraction of soil structure are induced by the high effective confining pressure.

Figure 9 shows the cohesion and the internal friction angle versus the hydrate saturation for HBS. As the hydrate saturation increases, the cohesion tends to significantly increase, and the internal friction angle almost remains unchanged. When the hydrate saturation increases from 0 to 32.9%, the cohesion is improved by 450% more or less. This result is consistent with the previous research results [7, 18, 35]. Miyazaki et al. [36] proposed an empirical formula to describe the change in cohesion with hydrate saturation. The similar formula is adopted to characterize the relationship between the cohesion and the hydrate saturation, shown in Figure 9. The great consistence between the fitting result and the experimental data shows the empirical formula proposed by Miyazaki et al. [36], which can reflect the influence of hydrate saturation on the cohesion of HBS. As for the internal friction angle, Masui et al. [37] found a consistent conclusion with this study, and the existence of hydrate did not affect the internal friction angle of HBS. However, Ghiassian and Grozic [28] found that the internal friction angle first increased slightly and then decreased with the increasing hydrate saturation. In fact, the slight increase or decrease in the internal friction angle with hydrate saturation can be neglected, and the hydrate saturation independent on the internal friction angle can be accepted.

4. Constitutive Model Development

4.1. Original Duncan–Chang Model. Since a great deal of stress-strain curves of soil specimens coincides with the hyperbolic curve, Duncan and Chang [38] proposed a Duncan–Chang constitutive model. In the Duncan–Chang constitutive model, the stress-strain curves satisfy the following relationship:

$$q = \frac{\varepsilon_1}{a + b\varepsilon_1}, \tag{3}$$

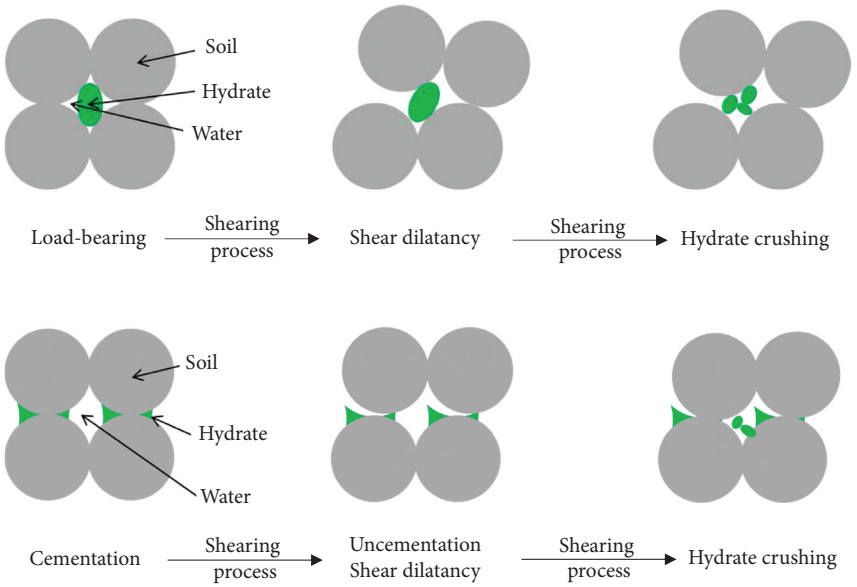

Figure 6: The mechanism for internal structure evolution of hydrate-bearing sediment during shearing [7, 28].

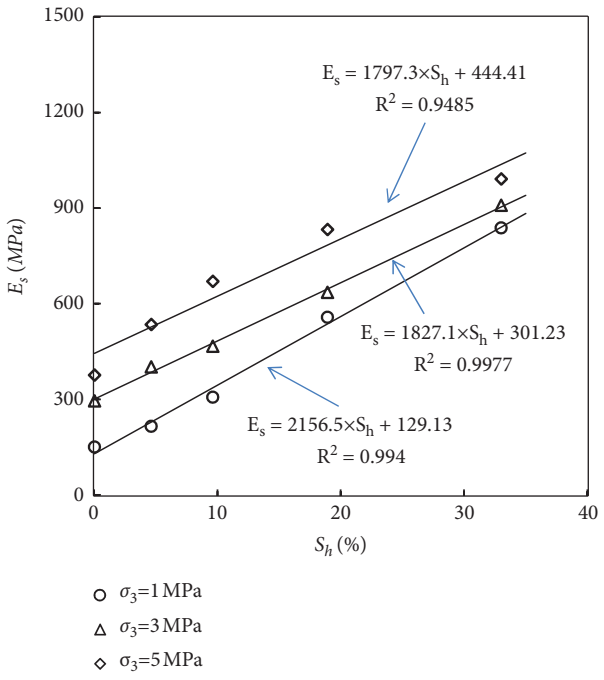

Figure 7: The relationships between the secant modulus and hydrate saturation.

where q is the deviatoric stress, ε_1 is the axial strain, a and b are model parameters, and the units are MPa^{-1}, related to the soil characteristics.

Parameter a is determined by the initial modulus of specimen, which can be expressed by

$$a = \frac{1}{E_i}, \tag{4}$$

where E_i is the initial modulus of specimen. Because of the influence of the effective confining pressure, Junbu [39] gives an empirical formula for the initial modulus

$$E_i = K \cdot \text{MPa} \cdot \left(\frac{\sigma_3'}{\text{MPa}}\right)^n, \tag{5}$$

where σ_3' is the effective confining pressure applying on the specimen, and K and n are model parameters.

Parameter b can be determined by the limit value q_{ult} of the asymptotic line of the deviatoric stress. The detailed expression can be expressed by

$$b = \frac{1}{q_{\text{ult}}}. \tag{6}$$

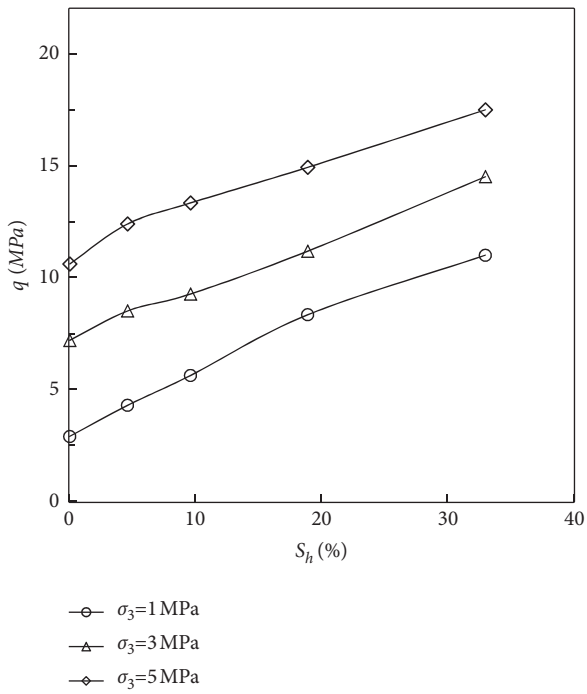

Figure 8: The relationship between failure strength and hydrate saturation.

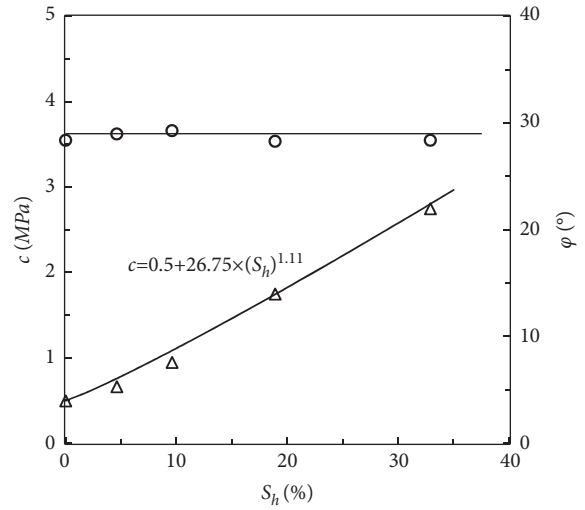

Figure 9: The cohesion and internal friction angle versus hydrate saturation for HBS.

Introducing the failure ratio $R_f = q_f/q_{ult}$, and q_f is the strength of the soil specimen. Thus, one can obtain the relationship between strength and parameter b as follows:

$$b = \frac{R_f}{q_f}. \tag{7}$$

Generally, the failure ratio is set to be 0.75–0.95 [40]. According to the Mohr-Coulomb strength criterion, the strength of the specimen can be obtained as

$$q_f = \frac{2c \cdot \cos\varphi + 2\sigma_3' \cdot \sin\varphi}{1 - \sin\varphi}, \tag{8}$$

where c and φ are cohesion and internal friction angle of the soil specimen. Based on equations (7) and (8), one can obtain the parameter b. Combining equations (4) and (5), the parameter a can be determined. Subsequently, the stress-strain curves can be calculated by equation (3).

4.2. The Modified Duncan–Chang Model. Hydrate formation could cement the soil particles and fill into the sediment pores. This change in the structure could increase the integrity of HBS, further causing the enhancement of stiffness and strength [7, 41]. Therefore, the parameters a and b can be influenced by the hydrate content.

For the hydrate-bearing sediments, the initial elastic modulus is affected by the hydrate saturation and the effective confining pressure. The original Duncan–Chang model satisfactorily addresses the effective confining pressure influence on the initial elastic modulus through equation (5), while the hydrate saturation influence is not considered. Lijith et al. [18] suggested a power function to relate an elastic modulus to hydrate saturation. Yan et al. [42] and Miyazaki et al. [25] developed a linear relationship between the elastic modulus and hydrate saturation, which has been used in the constitutive models, and obtained great simulated results. Moreover, Figure 6 shows the linear increase of the secant modulus with hydrate saturation. Herein, the authors adopt a linear function for the relationship of the initial elastic modulus and hydrate saturation

$$E_i = \left(E_i^0 + \delta \cdot S_h\right)\left(\frac{\sigma_3'}{MPa}\right)^{\chi}, \tag{9}$$

where E_i^0 is the initial elastic modulus of host sediment (unit: MPa), S_h is the hydrate saturation, and δ and χ are model parameters, which reflects the influences of hydrate and the effective confining pressure on the initial elastic modulus. The unit of δ is MPa.

To address the influence of hydrate cementation on the strength, some investigators adopted the power function to relate the increased part of the strength to the hydrate saturation [18, 25] and proposed the following formula for the strength of the hydrate-bearing sediment:

$$q_f = \frac{2 \cdot \cos\varphi}{1 - \sin\varphi}c_0 + \frac{2\sin\varphi}{1 - \sin\varphi}\sigma_3' + \alpha \cdot S_h^{\beta}, \tag{10}$$

where c_0 and φ are the cohesion and internal friction angle for host sediment. α and β are the model parameters, which are used to control the influence tendency of hydrate saturation on strength. In equation (10), the first two terms represent the contributions of soil skeleton to strength, and the third term considers the contribution of hydrate saturation. Clearly, equation (10) ignores the influence of hydrate saturation on the internal friction angle and suggests that the enhanced strength of HBS mainly results from the increasing cohesion.

In the constitutive model of HBS, the test parameter a can be obtained by replacing equation (9) with equation (4). With equation (10) instead of equation (7), the test parameter b can be obtained. It should be noted that the strain-softening behavior of HBS cannot be reflected if the test parameters and equation (3) are directly used to predict the stress-strain relationship of HBS. This is because the effects of hydrate damage and fragmentation during shearing process are not taken into account in the model. Therefore, equation (7) is modified here and the strength q_f' after the damage of the specimen is used instead of q_f. That is,

$$b = \frac{R_f}{q_f'}, \tag{11a}$$

$$q_f' = q_f(1 - D), \tag{11b}$$

where D is the damage factor. Equation (11b) mainly considers the decrease of the strength of HBS caused by hydrate damage and fragmentation during the shearing process , which leads to the change of the test parameter b.

During the process of shear, if the shear strength is less than the failure strength, the damage of the sample is small, and it is considered that there is no damage, $D = 0$. When the peak strength is reached, the shear action will gradually lead to structural damage, and the damage will gradually increase, resulting in a decrease in the strength of the sample. In order to describe the evolution of the damage factor with the shear process, the following formula is assumed to determine the relationship between the damage factor and the axial strain:

$$D = 1 - \exp(-n\varepsilon_1), \tag{12}$$

where ε_1 is the axial strain increment after the peak strength, and n is the model parameter, which mainly controls the change rate of the damage factor with axial strain.

The existing experimental results show that the increase of hydrate saturation will enhance the strain-softening behavior of HBS, while the increase of confining pressure will inhibit the strain-softening behavior. Therefore, the parameter n will be affected by confining pressure and hydrate saturation. To describe this effect, a simple empirical relationship is assumed,

$$n = \langle k_1 S_h - k_2\left(\frac{\sigma_3'}{\text{MPa}}\right) + n_0\rangle, \tag{13}$$

where is the MaCaulay bracket , $\langle x\rangle = x$ for $x \geq 0$, and $\langle x\rangle = 0$ for $x < 0$; k_1, k_2, and n_0 are model parameters. k_1 and k_2 control the effects of hydrate saturation and confining pressure on the model parameter n, respectively. The increase of hydrate saturation leads to the increase of the model parameter n, and the model shows the increased hydrate damage breaking effect, which leads to the enhancement of strain softening. While the increase of confining pressure leads to the decrease of the model parameter n, the model shows the reduced hydrate damage breaking effect, which weakens the strain-softening behavior. It is worth noting that the denser soil may still show a strain-softening behavior under low confining pressure when the hydrate saturation is 0%, so the model parameter n_0 is set in equation (13). If the soil without hydrate shows a strain-hardening behavior, then the model parameter $n_0 = 0$.

Table 2: Model parameters.

Parameter	Value
E_i^0 (MPa)	200
δ (MPa)	5000
χ	0.15
c_0 (MPa)	0.49
φ (°)	28.8
R_f	0.80
α (MPa)	26.75
β	1.11
k_1	10
k_2	0.95
n_0	4.0

Based on the above work, the parameter a is obtained according to equations (4) and (9), and the parameter b is obtained by using equation (11). Then, the stress-strain curves of HBS can be predicted by using the obtained model parameters and equation (3).

4.3. Model Verification and Analysis. This section is used to validate and analyze the modified Duncan–Chang model. The model parameters of this model mainly include E_i^0, c_0, φ, R_f, α, β, χ, k_1, k_2, and n_0. Among them, parameters E_i^0, c_0, φ, and R_f are the mechanical properties of host sediments, which can be determined according to the stress-strain curves of host sediments. The determination of other parameters can be determined by fitting the stress-strain curves of hydrate-bearing sediment samples with different hydrate saturations and different confining pressures. To verify the constitutive model, the experimental data for four different hydrate-bearing sediment samples are employed to compare the simulated results. Except for the stress-strain curve of hydrate-bearing fine sand in this paper, the stress-strain curves for the hydrate-bearing Toyoura sand, hydrate-bearing sediment in the South China Sea, and hydrate-bearing sediment in the Nankai Trough are involved.

4.3.1. Hydrate-Bearing Fine Sand. This study performed the triaxial compression tests on the methane hydrate-bearing fine sand with the effective confining pressures of 1, 3, and 5 MPa. Under these effective confining pressures, the mechanical behaviors of hydrate-bearing fine sand with different hydrate saturations are analyzed. Adopting the modified Duncan–Chang model, we calculate the stress-strain curves and compare to the experimental data. The used model parameters are shown in Table 2.

Figure 10 shows the comparison between the calculated and measured stress-strain curves for the hydrate-bearing fine sand with different hydrate saturations under different effective confining pressures of 1, 3, and 5 MPa. The good agreement between the simulated result and experimental data shows that the modified Duncan–Chang model can effectively capture the fundamental mechanical behaviors of

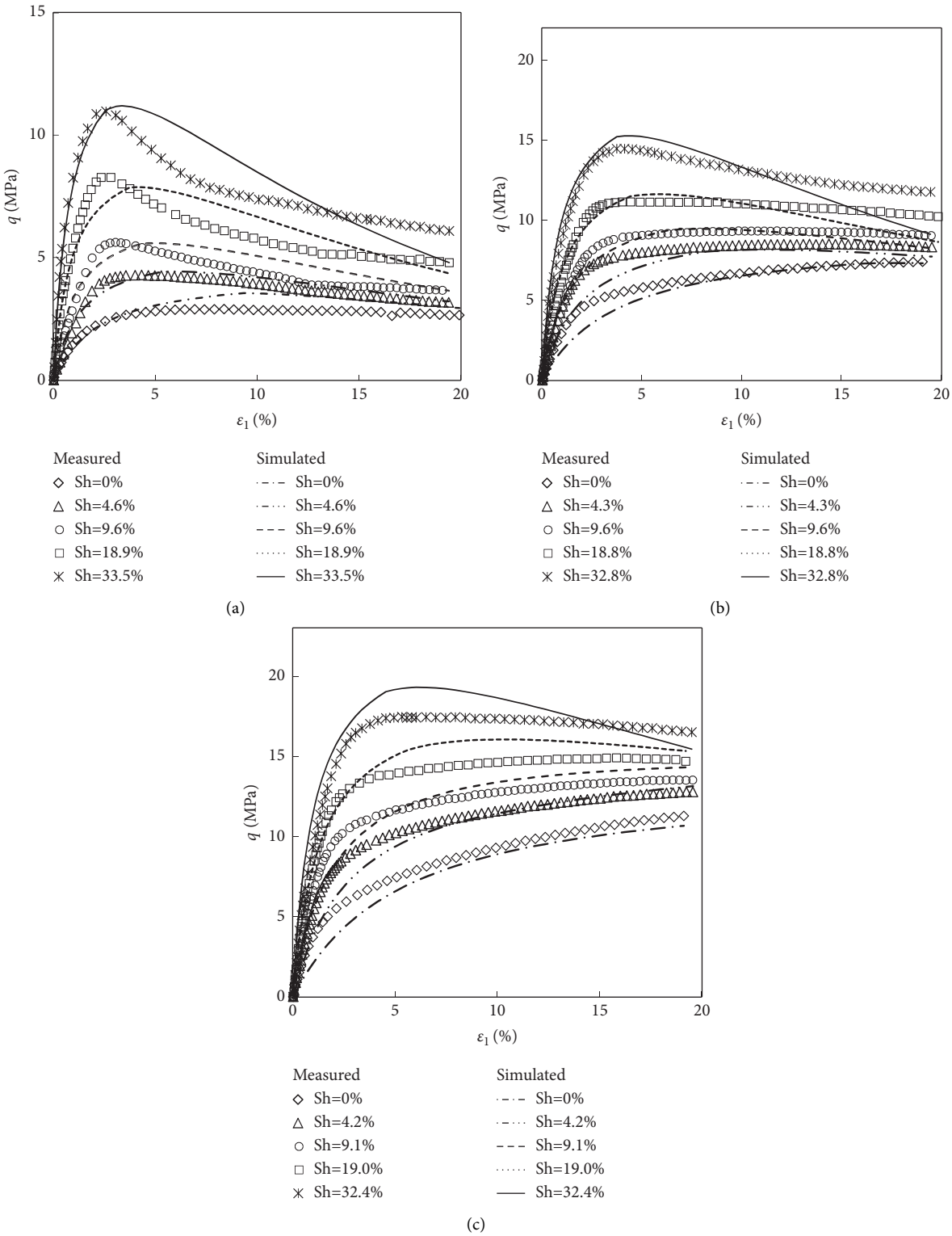

Figure 10: Comparisons of the calculated and experimental stress-strain curves for HBS: (a) $\sigma_3' = 1$ MPa, (b) $\sigma_3' = 3$ MPa, and (c) $\sigma_3' = 5$ MPa.

methane hydrate-bearing fine sand. Due to the influence of the hydrate cementation effect, the strength and stiffness of the sample increase significantly with the increasing hydrate saturation. The constitutive model satisfactorily reflects the influences of hydrate saturation on the stiffness and strength of methane hydrate-bearing fine sand. Moreover, the strain-softening characteristics of the sample are properly addressed by the modified Duncan–Chang model. The

Table 3: Model parameters.

Parameter	Value
E_i^0 (MPa)	350
δ (MPa)	5000
χ	0.15
c_0 (MPa)	0.49
φ (°)	31.0
R_f	0.9
α (MPa)	17
β	2.35
k_1	10
k_2	1.2
n_0	1.8

Table 4: Model parameters.

Parameter	Value
E_i^0 (MPa)	350
δ (MPa)	4500
χ	0.15
c_0 (MPa)	1.13
φ (°)	26
R_f	0.8
α (MPa)	800
β	4.2
k_1	6
k_2	0.95
n_0	3

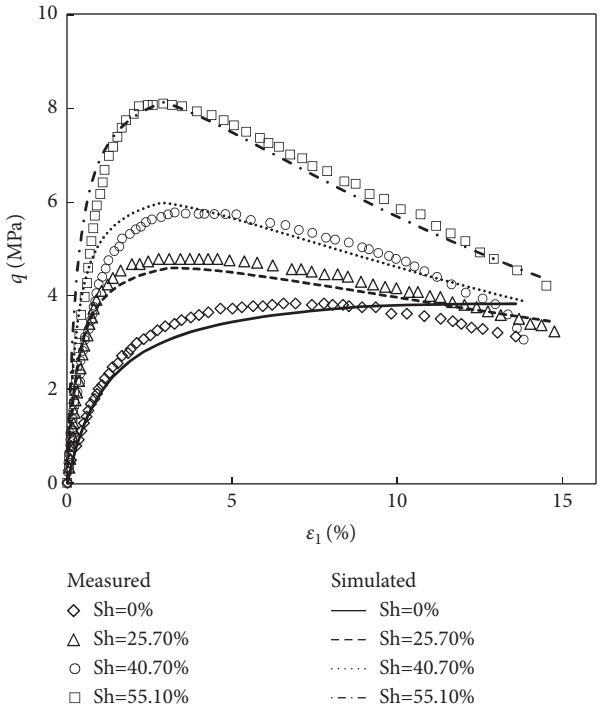

Figure 11: Comparisons between the simulated result and experimental data for hydrate-bearing Toyoura sand [35].

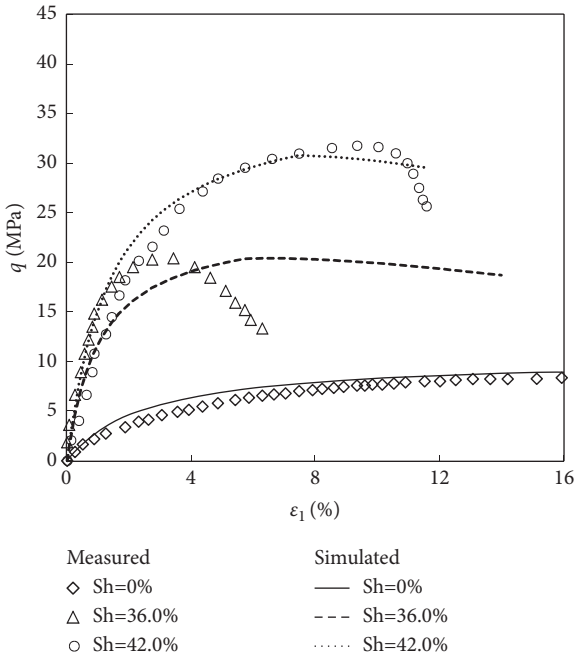

Figure 12: Comparisons of the calculated and experimental stress-strain curves for the hydrate-bearing sediment in the South China Sea [43].

higher hydrate saturation gives rise to the more obvious strain-softening behaviors, but the increasing effective confining pressure hinders the strain-softening characteristic of HBS.

4.3.2. Hydrate-Bearing Toyoura Sand. In this section, the methane hydrate-bearing Toyoura sand is used to verify the modified Duncan–Chang constitutive model. Masui et al. [37] used Toyoura sand as host sediment and adopted the water-sand mixing and ice-sand mixing method to synthesize HBS at low temperature in a gas-rich environment. During the shear process, the pore methane gas pressure is 8.0 MPa and the temperature is 278 K. To validate the capacity of addressing the enhanced stiffness, strength, and strain-softening characteristics of HBS, the modified Duncan–Chang model simulates the stress-strain curves of methane hydrate-bearing sand prepared by the water-sand mixing method under the different hydrate saturation cases. The effective confining pressure is set to be 1 MPa. The model parameters adopted in the simulation are shown in Table 3.

Figure 11 presents the calculated and experimental stress-strain relationship for methane hydrate-bearing sand with different hydrate saturations under 1 MPa effective confining pressure. It can be seen from Figure 10 that the model calculation curve is in good agreement with the test curve, indicating that the model can effectively reflect the effect of hydrate saturation on the mechanical properties of HBS. With the increase of hydrate saturation, the cementation effect is enhanced, causing the increase of strength and stiffness of the specimen. As known, the water-sand mixing method reproduces the hydrate within sediment pores with cementing habits. The hydrate often exists at the contact surface between the soil particles; thus a small

Table 5: Model parameters.

Parameter	Value		
	No. 7 & No. 7-2	No. 8 & No. 8-2	No. 9 & No. 9-2
E_i^0 (MPa)	60	200	200
δ (MPa)	500	700	1500
χ	0.2	0.15	0.15
c_0 (MPa)	0.05	0.11	0.1
φ (°)	29	34.7	34
R_f	0.85	0.75	0.85
α (MPa)	25.5	16.7	10
β	2.53	2.69	1.8
k_1	10	9.5	10
k_2	0	1	2.5
n_0	0	0.5	1

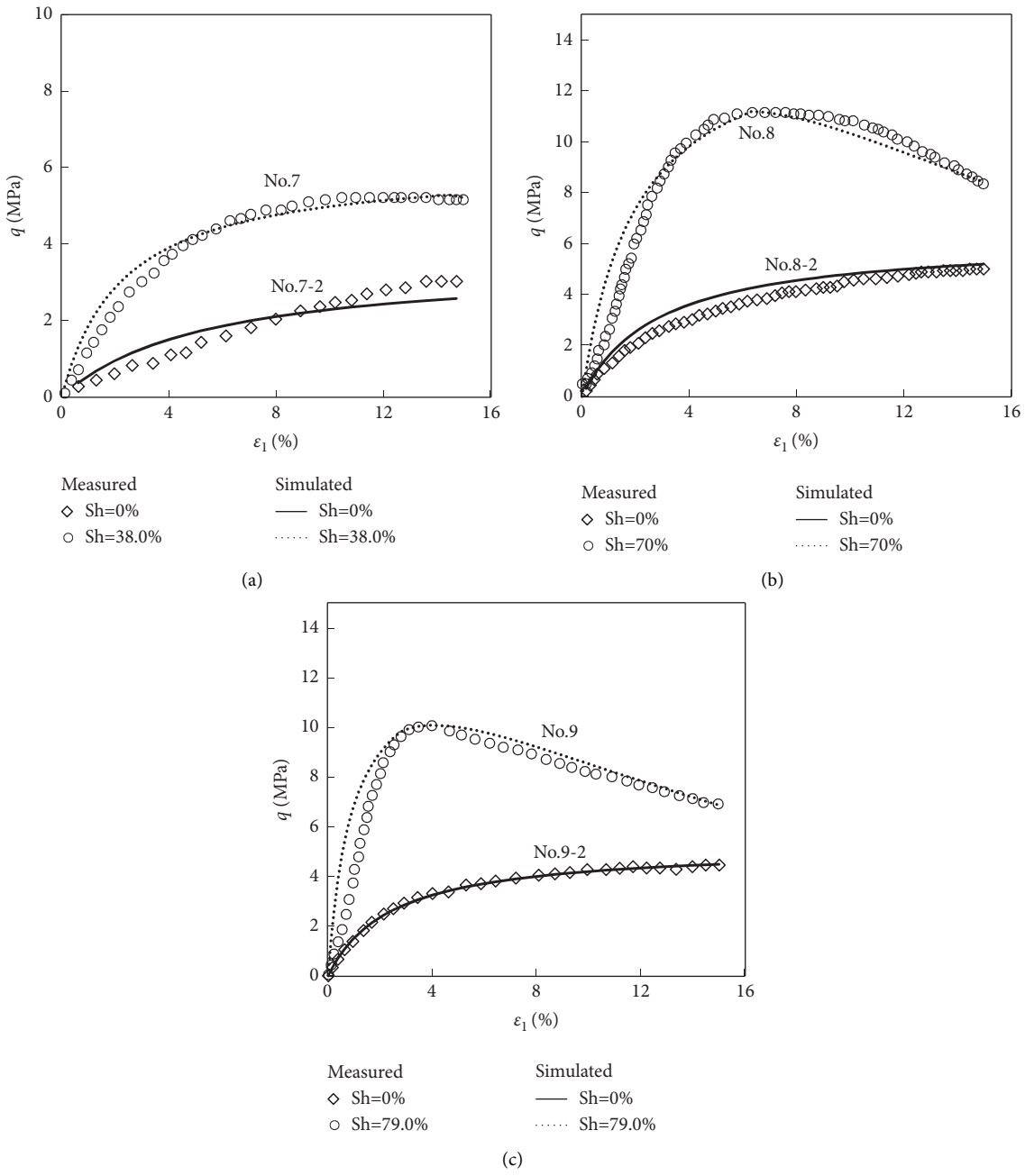

Figure 13: Comparisons between the calculated and experimental results for HBS in the Nankai Trough, Japan [14]: (a) No. 7 and No. 7-2, (b) No. 8 and No. 8-2, and (c) No. 9 and No. 9-2.

amount of hydrate content can cause the significant improvement in the stiffness and strength of HBS. The simulated stress-strain curves properly capture this stiffness and strength dependence on hydrate saturation of HBS. In addition, the simulated result also illustrates the more obvious strain-softening behavior at higher hydrate saturation. Therefore, it can be demonstrated that the modified Duncan–Chang model can not only simulate the enhanced stiffness and strength characteristics of methane hydrate-bearing sand sample but also effectively capture the strain-softening behavior of the methane hydrate-bearing sand sample.

4.3.3. HBS in the South China Sea. Xie et al. [43] used sand from hydrate-bearing strata in the South China Sea as sediments to form HBS by the excess gas method, and the triaxial shear tests were performed. The applied effective confining pressure is 3 MPa. The pore pressure of 12 MPa and the temperature of 275 K provided the environment for methane hydrate stable during the shear test. Using the model parameters listed in Table 4, which is calibrated through the stress-strain curve with Sh = 0 and 42%, the proposed modified Duncan–Chang model simulated the stress-strain curves of HBS in the South China Sea.

Figure 12 shows the comparison between the calculated result and experimental data for HBS in the South China Sea. From Figure 11, it can be seen from that the modified Duncan–Chang model can simulate the stress-strain curve of HBS with $S_h = 42.0\%$ well. Meanwhile, the proposed model can also effectively capture the strain-softening characteristic of the HBS sample. For the HBS sample with $S_h = 36.0\%$, however, the simulated result slightly deviates from the experimental data. Comparing the stress-strain curve of $S_h = 36\%$ to $S_h = 42\%$, it is found that the initial modulus for $S_h = 36\%$ is higher than that for $S_h = 42\%$, which is apparently unreasonable. Therefore, it is reasonable to believe that there is a structural difference in the HBS sample between $S_h = 36\%$ and $S_h = 42\%$. When we use the model parameters calibrated by the case of $S_h = 42\%$, it is inevitable to give rise to the large discrepancy between the calculated and experimental stress-strain relationship for the HBS sample with $S_h = 36\%$.

4.3.4. HBS in Nankai Trough. To reveal the mechanical properties of HBS in Nankai Trough sea area, Yoneda et al. [14] carried out the triaxial compression tests on the HBS samples drilled from the Nankai Trough. This paper chose the drainage triaxial compression test results of No. 7, No. 7-2, No. 8, No. 8-2, and No. 9, No. 9-2 to verify the proposed model. The samples of No. 7, No. 8, and No. 9 are silty sand with hydrate saturation of 38%, 70%, and 79%, respectively. The samples of No. 7-2, No. 8-2, and No. 9-2 are remolded to measure the mechanical behaviors of the hydrate-free sediments for comparison. In the triaxial compression tests, the effective confining pressures of No. 7 and No. 7-2 are 1.5 MPa, and the effective confining pressures of No. 8, No. 8-2 and No. 9, No. 9-2 are 1.6 MPa. In the simulation, the used model parameters are shown in Table 5.

Figure 13 shows the calculated and experimental results for the stress-strain curves of HBS and pure sediment from the Nankai Trough sea area. It is obvious that the stiffness and strength of HBS are significantly higher than those of hydrate-free sediment, which mainly results from the hydrate cementation effect for soil particles. Figure 12 also finds that the samples of No. 7, No. 8, and No. 9 show completely different stress-strain behaviors. The No. 7 sample shows an obvious strain-hardening stress-strain curve, while the samples of No. 8 and No. 9 show an obvious strain-softening behavior. The modified Duncan–Chang model properly addresses these two completely different mechanical behaviors of HBS. Apparently, the proposed model can not only effectively simulate the strain-hardening behaviors of HBS but also satisfactorily reflect the strain-softening behaviors of HBS.

5. Conclusions

This paper performed several triaxial compression tests on the hydrate-bearing sand sediment to study the mechanical properties of sediment containing different hydrate contents. The enhanced stiffness, strength, and strain-softening characteristics of HBS are analyzed. Based on the experimental result of the previous research achievements, the Duncan–Chang model is extended to simulate the stress-strain relationship of HBS, especially for the strain-softening behaviors.

(1) Since the hydrate cements the soil skeleton of sediment, the stiffness and strength increase with the increasing hydrate saturation. The enhanced strength mainly results from the increase in the cohesion of HBS. The internal friction angle is independent of the hydrate saturation. The linear expression could be used to describe the relation of the modulus and hydrate saturation, and the power function is able to characterize the change in strength with the hydrate saturation.

(2) The hydrate-bearing sand sediment exhibits a remarkable strain-softening behavior, which is related to the hydrate saturation and the effective confining pressure. As the hydrate saturation increases, and/or the effective confining pressure decreases, the strain-softening behavior is more obvious. A new concept parameter, strain-softening index, is introduced to quantitatively analyze the softening characteristics of HBS, which satisfactorily reflects the influences of hydrate saturation and effective confining pressure on the strain-softening properties of HBS. In addition, the analysis on the microscopic mechanism reveals that hydrate damage and fragmentation are critical reasons for the strain-softening behavior of HBS.

(3) The damage factor is introduced into the Duncan–Chang model to describe the damage law of HBS samples during shear, and a modified Duncan–Chang constitutive model of HBS is established. Compared with the experimental data, the modified

Duncan–Chang model can effectively simulate the stress-strain curves of HBS, which can not only consider the effect of hydrate occurrence on strength and stiffness but also effectively describe the strain-softening behaviors of HBS.

(4) The establishment of the modified Duncan–Chang model of HBS considering the strain-softening effect provides an important reference for extending the application of the Duncan–Chang model to the other soils with the strain-softening characteristic.

Data Availability

The data presented in this study are available on request from the first author or the corresponding author.

Ethical Approval

Not applicable.

Consent

Not applicable.

Conflicts of Interest

The authors declare no conflicts of interest.

Authors' Contributions

M.Y. and R.Y. designed the experiments and interpreted the results; M.Y. performed the experiments; and M.Y., H.Y., and R.Y. analyzed the data and wrote the paper. All authors have read and agreed to the published version of the manuscript.

Acknowledgments

This research was funded by the National Natural Science Foundation of China (11962004 and 11562007).

References

[1] K. A. Kvenvolden and T. D. Lorenson, "The global occurrence of natural gas hydrate," *Geophysical Monograph Series*, vol. 124, pp. 3–18, 2001.

[2] R. A. Dawe and S. Thomas, "A large potential methane source - natural gas hydrates," *Energy Sources, Part A: Recovery, Utilization, and Environmental Effects*, vol. 29, no. 3, pp. 217–229, 2007.

[3] Q. Bu, G. Hu, C. Liu, T. Xing, C. Li, and Q. Meng, "Acoustic characteristics and micro-distribution prediction during hydrate dissociation in sediments from the South China Sea," *Journal of Natural Gas Science and Engineering*, vol. 65, pp. 135–144, 2019.

[4] Y. F. Makogon, "Natural gas hydrates-A promising source of energy," *Journal of Natural Gas Science and Engineering*, vol. 2, no. 1, pp. 49–59, 2010.

[5] R. Boswell and T. S. Collett, "Current perspectives on gas hydrate resources," *Energy & Environmental Science*, vol. 4, no. 4, pp. 1206–1215, 2011.

[6] N. Sultan, J. Cochonat, J. P. Foucher, and J. Mienert, "Effect of gas hydrates melting on seafloor slope instability," *Marine Geology*, vol. 213, no. 1, pp. 379–401, 2004.

[7] W. F. Waite, J. C. Santamarina, D. D. Cortes et al., "Physical properties of hydrate-bearing sediments," *Reviews of Geophysics*, vol. 47, no. 4, pp. 465–484, 2009.

[8] M. Hyodo, Y. Li, J. Yoneda et al., "Mechanical behavior of gas-saturated methane hydrate-bearing sediments," *Journal of Geophysical Research: Solid Earth*, vol. 118, no. 10, pp. 5185–5194, 2013.

[9] T. S. Yun, J. C. Santamarina, and C. Ruppel, "Mechanical properties of sand, silt, and clay containing tetrahydrofuran hydrate," *J. Geophys. Res. Solid Earth*, vol. 112, no. B4, Article ID B04106, 2007.

[10] Y. Wu, J. Cui, J. Huang, W. Zhang, N. Yoshimoto, and L. Wen, "Correlation of critical state strength properties with particle shape and surface fractal dimension of clinker ash," *International Journal of Geomechanics*, vol. 21, no. 6, Article ID 04021071, 2021.

[11] B. Yuan, Z. Li, Z. Zhao, H. Ni, Z. Su, and Z. Li, "Experimental study of displacement field of layered soils surrounding laterally loaded pile based on Transparent Soil," *Journal of Soils and Sediments*, vol. 21, no. 9, pp. 3072–3083, 2021.

[12] S. Kimoto, F. Oka, T. Fushita, and M. Fujiwaki, "A chemo-thermo-mechanically coupled numerical simulation of the subsurface ground deformations due to methane hydrate dissociation," *Computers and Geotechnics*, vol. 34, no. 4, pp. 216–228, 2007.

[13] X. Sun, L. Wang, H. Luo, Y. Song, and Y. Li, "Numerical modeling for the mechanical behavior of marine gas hydrate-bearing sediments during hydrate production by depressurization," *Journal of Petroleum Science and Engineering*, vol. 177, pp. 971–982, 2019.

[14] J. Yoneda, A. Masui, Y. Konno et al., "Mechanical properties of hydrate-bearing turbidite reservoir in the first gas production test site of the Eastern Nankai Trough," *Marine and Petroleum Geology*, vol. 66, pp. 471–486, 2015.

[15] Z. Liu, S. Dai, F. Ning, L. Peng, H. Wei, and C. Wei, "Strength estimation for hydrate-bearing sediments from direct shear tests of hydrate-bearing sand and silt," *Geophysical Research Letters*, vol. 45, 2018.

[16] J. Yoneda, M. Oshima, M. Kida et al., "Consolidation and hardening behavior of hydrate-bearing pressure-core sediments recovered from the Krishna-Godavari Basin, offshore India," *Marine and Petroleum Geology*, vol. 108, pp. 512–523, 2019.

[17] M. Hyodo, Y. Wu, K. Nakashima, S. Kajiyama, and Y. Nakata, "Influence of fines content on the mechanical behavior of methane hydrate-bearing sediments," *Journal Geophysical Research Solid Earth*, vol. 108, 2017.

[18] K. P. Lijith, B. R. C. Malagar, and D. N. Singh, "A comprehensive review on the geomechanical properties of gas hydrate bearing sediments," *Marine and Petroleum Geology*, vol. 104, pp. 270–285, 2019.

[19] S. Uchida, K. Soga, and K. Yamamoto, "Critical state soil constitutive model for methane hydrate soil," *J. Geophys. Res. Solid Earth*, vol. 117, no. B3, 2012.

[20] X. Sun, X. Guo, L. Shao, and H. Tang, "A thermodynamics-based critical state constitutive model for methane hydrate bearing sediment," *Journal of Natural Gas Science and Engineering*, vol. 27, pp. 1024–1034, 2015.

[21] J. Shen, C. F. Chiu, C. W. W. Ng, G. H. Lei, and J. Xu, "A state-dependent critical state model for methane hydrate-bearing

sand," *Computers and Geotechnics*, vol. 75, no. 5, pp. 1–11, 2016.

[22] R. Yan and C. Wei, "Constitutive model for gas hydrate-bearing soils considering hydrate occurrence habits," *International Journal of Geomechanics*, vol. 17, no. 8, Article ID 4017032.1, 2017.

[23] M. Sánchez, X. Gai, and J. Santamarina, "A constitutive mechanical model for gas hydrate bearing sediments incorporating inelastic mechanisms," *Computers and Geotechnics*, vol. 84, pp. 28–46, 2017.

[24] K. Miyazaki, K. Aoki, N. Tenma, Y. Sakamoto, and T. Yamaguchi, "Application of nonlinear elastic constitutive model to analysis of artificial methane-hydrate-bearing sediment sample," in *Proceedings of the ninth ISOPE Ocean Mining Symposium*, pp. 19–24, Maui, HA, USA, June 2011.

[25] K. Miyazaki, N. Tenma, K. Aoki, and T. Yamaguchi, "A nonlinear elastic model for triaxial compressive properties of artificial methane-hydrate-bearing sediment samples," *Energies*, vol. 5, no. 10, pp. 4057–4075, 2012.

[26] F. Yu, Y. Song, Y. Li, W. Liu, and W. Lam, "Analysis of stress-strain behavior and constitutive relation of methane hydrate-bearing sediments with various porosity," *International Journal of Offshore and Polar Engineering*, vol. 21, no. 4, pp. 316–322, 2011.

[27] Y. Song, Y. Zhu, W. Liu, Y. Li, Y. Lu, and Z. Shen, "The effects of methane hydrate dissociation at different temperatures on the stability of porous sediments," *Journal of Petroleum Science and Engineering*, vol. 147, pp. 77–86, 2016.

[28] H. Ghiassian and J. L. H. Grozic, "Strength behavior of methane hydrate bearing sand in undrained triaxial testing," *Marine and Petroleum Geology*, vol. 43, pp. 310–319, 2013.

[29] T. Luo, Y. Li, B. N. Madhusudhan, J. Zhao, and Y. Song, "Comparative analysis of the consolidation and shear behaviors of CH4 and CO2 hydrate-bearing silty sediments," *Journal of Natural Gas Science and Engineering*, vol. 75, Article ID 103157, 2020.

[30] A. Kumar, T. Sakpal, S. Roy, and R. Kumar, "Methane hydrate formation in a test sediment of sand and clay at various levels of water saturation," *Canadian Journal of Chemistry*, vol. 93, no. 3, pp. 1742–1773, 2015.

[31] B. Madhusudhan, C. Clayton, and J. Priest, "The effects of hydrate on the strength and stiffness of some sands," *Journal of Geophysical Research Solid Earth*, vol. 124, pp. 65–75, 2019.

[32] Ministry of Water Resources of the People's Republic of China, *Standard for geotechnical testing method GB/T 50123-2019*, China Planning Press, Beijing, China, 2019.

[33] R. Yan, C. Wei, H. Wei, H. Tian, and E. Wu, "Effect of hydrate formation on mechanical strength of hydrate-bearing sand," *Chinese Journal of Geotechnical Engineering*, vol. 34, no. 7, pp. 1234–1240, 2012.

[34] S. Pinkert, J. L. H. Grozic, and J. A. Priest, "Strain-softening model for hydrate-bearing sands," *International Journal of Geomechanics*, vol. 15, no. 6, Article ID 04015007, 2015.

[35] J. Zhou, Z. Yang, C. Wei, P. Chen, and R. Yan, "Mechanical behavior of hydrate-bearing sands with fine particles under isotropic and triaxial compression," *Journal of Natural Gas Science and Engineering*, vol. 92, Article ID 103991, 2021.

[36] K. Miyazaki, T. Yamaguchi, Y. Sakamoto, N. Tenma, Y. Ogata, and K. Aoki, "Effect of confining pressure on mechanical properties of sediment containing synthetic methane hydrate," *Journal of MMIJ*, vol. 126, no. 7, pp. 408–417, 2010.

[37] A. Masui, H. Haneda, Y. Ogata, and K. Aoki, "Effects of methane hydrate formation on shear strength of synthetic methane hydrate sediments," in *Proceedings of the Fifteenth International Offshore and Polar Engineering Conference*, pp. 19–24, Seoul, Korea, June 2005.

[38] J. M. Duncan and C.-Y. Chang, "Nonlinear analysis of stress and strain in soils," *Journal of the Soil Mechanics and Foundations Division*, vol. 96, no. 5, pp. 1629–1653, 1970.

[39] N. Janbu, "Soil Compressibility as determined by oedometer and triaxial test," in *Proceedings of the Third European Conference on Soil Mechanics and Foundation Engineering*, pp. 19–25, Wiesbaden, Germany, 1963.

[40] T. Luo, Y. Yao, and W. Hou, *Soil Constitutive Models*, pp. 65–67, China Communications Press, Beijing, China, 2010.

[41] A. Masui, K. Miyazaki, H. Haneda, Y. Ogata, and K. Aoki, "Mechanical characteristics of natural and artificial gas hydrate bearing sediments," in *Proceedings of the Sixth International Conference on Gas Hydrates (ICGH 2008)*, pp. 6–10, Vancouver, Canada, July 2008.

[42] R. Yan, B. Zhang, D. Yang, Y. Li, X. Chen, and C. Wei, "Damage constitutive relation of hydrate-bearing sediments under different temperature-pressure conditions," *Rock and Soil Mechanics*, vol. 39, no. 12, pp. 4421–4428, 2018.

[43] X. G. Xie, Y. F. Leung, S. Uchida, J. S. Lu, D. L. Li, and D. Q. Liang, "Experimental and Numerical Studies on Geomechanical Behavior of Various Gas Hydrate-Bearing Sediments in China," in *Proceedings of the First International Conference on Energy Geotechnics*, pp. 29–31, Kiel, Germany, August 2016.